João Elias F. S. Rodrigues, Javier Gainza, Federico Serrano-Sánchez, Norbert M. Nemes, Oscar J. Dura, Jose Luis Martínez and Jose Antonio Alonso*

A novel crystallographic location of rattling atoms in filled $Eu_xCo_4Sb_{12}$ skutterudites prepared under high-pressure conditions

https://doi.org/10.1515/zkri-2022-0051
Received August 30, 2022; accepted November 14, 2022; published online December 12, 2022

Abstract: Thermoelectric $M_xCo_4Sb_{12}$ skutterudites are well-known to exhibit a reduced thermal conductivity thanks to the rattling effect of the M-filler at the large cages occurring in the framework, centered at the 2*a* sites of the $Im\bar{3}$ space group. A novel Eu-filled skutterudite has been synthesized under high-pressure conditions at 3.5 GPa in a piston-cylinder hydrostatic press. The structural refinement from high-angular resolution synchrotron X-ray diffraction (SXRD) patterns unveils an unusual position for Eu filler atoms. By difference Fourier synthesis they are found at 12*d* sites, conforming statistically occupied octahedra within the mentioned cages around 2*a* positions. The Debye temperature was estimated by averaging the isotropic displacements by the atomic masses, leading to θ_D of 273(2) K. Oftedal plots concerning the *y* and *z* Sb fractional positions, the unit-cell parameter ***a*** and M filling fraction include the novel Eu specimen in the trend observed for other filled materials prepared under high-pressure, including rare-earths, alkali or alkali-earth elements, all accepted as rattlers in filled skutterudites. A total thermal conductivity (κ) of 0.82 W m^{-1} K^{-1} is measured at 773 K for $Eu_{0.02(1)}Co_4Sb_{12}$, below that of other filled skutterudites, which is promoted by the enhanced phonon scattering of Eu located at 12*d* sites. FE-SEM images showed large, homogeneous grains, well compacted after the high-pressure synthesis.

Keywords: filled skutterudites; synchrotron X-ray powder diffraction; thermal conductivity reduction; thermoelectrics.

***Corresponding author: Jose Antonio Alonso**, Instituto de Ciencia de Materiales de Madrid (ICMM), Consejo Superior de Investigaciones Científicas (CSIC), Sor Juana Inés de la Cruz 3, E-28049, Madrid, Spain, E-mail: ja.alonso@icmm.csic.es. https://orcid.org/0000-0001-5329-1225

João Elias F. S. Rodrigues, Instituto de Ciencia de Materiales de Madrid (ICMM), Consejo Superior de Investigaciones Científicas (CSIC), Sor Juana Inés de la Cruz 3, E-28049, Madrid, Spain; and European Synchrotron Radiation Facility (ESRF), 71 Avenue des Martyrs, 38000 Grenoble, France, E-mail: rodrigues.joaoelias@gmail.com. https://orcid.org/0000-0002-9220-5809

Javier Gainza, Federico Serrano-Sánchez and Jose Luis Martínez, Instituto de Ciencia de Materiales de Madrid (ICMM), Consejo Superior de Investigaciones Científicas (CSIC), Sor Juana Inés de la Cruz 3, E-28049, Madrid, Spain, E-mail: jgainza@ucm.es (J. Gainza), fserrano@icmm.csic.es (F. Serrano-Sánchez), martinez@icmm.csic.es (J.L. Martínez). https://orcid.org/0000-0002-1999-3116 (J. Gainza). https://orcid.org/0000-0002-6882-225X (F. Serrano-Sánchez). https://orcid.org/0000-0001-9046-8237 (J.L. Martínez)

Norbert M. Nemes, Departamento de Física de Materiales, Universidad Complutense de Madrid, E-28040 Madrid, Spain, E-mail: nmnemes@fis.ucm.es. https://orcid.org/0000-0002-7856-3642

Oscar J. Dura, Departamento de Física Aplicada, Universidad de Castilla-La Mancha, Ciudad Real, E-13071, Spain, E-mail: Oscar.Juan@uclm.es. https://orcid.org/0000-0002-4014-7555

1 Introduction

A strong motivation for researching within the appealing field of Thermoelectric Materials (TM) is that about two thirds of energy production (at a global level) is dissipated as heat with no profit. Yet, TMs are able to directly transform a thermal gradient into electric energy [1–4]. Designing novel TMs is challenging since three antagonistic properties must be optimized: they require high Seebeck voltages (*S*, thermoelectric power), low electrical resistivity (ρ), and low thermal conductivity (κ). TMs are typically semiconductors and so ρ is coupled to κ through the electronic contribution, κ_e, since the same carriers are involved in both mechanisms, and to their *S* due to the Pisarenko relation. TMs are characterized by a dimensionless Figure of Merit ($ZT = S^2T/\rho\kappa$); the best ZTs are around 1–2, depending on temperature (*T*). Currently, commercial TMs are made of chalcogenide semiconductors like PbTe or Bi_2Te_3. Both contain Te; a scarce and expensive element (one part per billion on earth crust).

Instead of chalcogenides, some metal pnictides perform well as TMs, in particular AX_3 skutterudites. They derive their name from the mineral $CoAs_3$; the structure

can host different transition metals (Fe, Co, Rh, Ir…) at A position, and pnictide elements (P, As, Sb) as X atoms [3]. Skutterudites are cubic, defined in the space group $Im\overline{3}$ [5]. A conspicuous feature is the existence of relatively large voids at 2*a* Wyckoff sites that can be filled with additional atoms. Filled skutterudites may contain lanthanide, alkali-earth or even alkali ions interstitially occupying these voids [6–8], with large thermal vibration parameters, indicating that they can "rattle" or participate in a soft phonon mode of the crystal structure. According to the PGEC theory (phonon-glass, electron-crystal) materials [9–11], this "ball in a cage" configuration of filled skutterudites directly determines the basic conditions for high ZT values: the effect of the atomic void fillers in oversized cages drastically reduces κ and thereby maximizes ZT. In earlier works, we have successfully synthesized and characterized such compounds. For instance, $CoSb_3$ can be stabilized at 3.5 GPa, finding exceptionally low thermal conductivities that were ascribed to partial antimony deficiency, the Sb vacancies acting as phonon scatterers [12]. We also synthesized $La_xCo_4Sb_{12}$, La being a rattler element [13]. Subsequently, other $M_xCo_4Sb_{12}$ pnictide skutterudites were filled with a panoply of rare-earths (Ce, Yb, Y, mischmetal), alkali earth (Sr) or alkali elements (K) [14–18], which were successfully stabilized in the 2*a* skutterudite cages.

Additionally, the structural analysis from high-angular resolution synchrotron X-ray diffraction (SXRD) unveils interesting features of these compounds. The so-called "Oftedal plots" [16], determined by the antimony positional parameters (*y* and *z*) as a function of the filling fraction, ionic state and atomic radius of the filler, yield an interesting view of the distortion of [Sb_4] rings contained in the structure, closely linked to the band-convergence concept and its influence on the thermoelectric transport properties [16–19].

Eu-filled skutterudites have been barely described since the first structural report on a compound $Eu_xCo_4Sb_{12}$ [20]. In this work, we describe a Eu-filled skutterudite, $Eu_xCo_4Sb_{12-\delta}$ prepared under high-pressure conditions, where high-angular resolution SXRD data disclosed a novel crystallographic position for the Eu rattling atoms, at 12*d* (*x*, 0, 0) sites, which combined with a conspicuous Sb deficiency leads to a substantial reduction of the thermal conductivity in this thermoelectric material.

2 Experimental procedures

A sample with nominal composition $Eu_{0.5}Co_4Sb_{12}$ was prepared by a solid-state reaction under moderate temperature and high-pressure conditions. About 1.2 g of a stoichiometric mixture of the starting elements Eu (99.0%), Co (99%, ROC/RIC), and Sb (99.5%, Alfa-Aesar) were carefully ground and placed in a niobium capsule (5 mm in diameter), sealed and introduced inside a cylindrical graphite heater. To prevent oxidation, the capsule was properly manipulated inside an Argon-filled glove box. Reactions were carried out in a piston-cylinder press (Rockland Research Co.), at a pressure of 3.5 GPa, at 800 °C for 1 h. Afterwards, the products were quenched to room temperature and the pressure was released. The samples were obtained as hard pellets, which were partially ground to powder for structural characterization, or cut with a diamond saw as bar-shaped pellets to perform transport measurements.

Phase characterization was carried out using X-ray diffraction (XRD) on a Bruker-AXS D8 diffractometer (40 kV, 30 mA), run by DIFFRACTPLUS software, in Bragg-Brentano reflection geometry with Cu Kα radiation (λ = 1.5418 Å). The structural details were analyzed from temperature-dependent SXRD patterns collected at the MSPD-diffractometer at the ALBA synchrotron (Barcelona, Spain), in the high-angular resolution mode (MAD set-up) with an incident beam of 27 keV energy (λ = 0.45861 Å) [21]. The polycrystalline powder was contained in rotating quartz capillaries of 0.7 mm in diameter. SXRD patterns were collected at room temperature (RT, 295 K), 473, 673, 873 and 1023 K for the temperature-dependent analysis. The *FullProf* software was used to refine the structure [22] with the Rietveld method [23]. The zero-point error, scale factor, background coefficients, pseudo-Voigt shape parameters, atomic coordinates, and anisotropic displacements for the Co and Sb atoms were refined.

The Seebeck coefficient was measured using a commercial MMR-technologies system. Measurements were performed under vacuum (10^{-3} mbar) from room temperature up to 800 K. A constantan wire was employed as a reference for comparison with bar-shaped skutterudite samples cut with a diamond saw perpendicular to the pressing direction. The reproducibility was checked with different contacts and constantan wires.

A Linseis LFA 1000 instrument was used to measure the thermal diffusivity (α) of the samples over a temperature range of $300 \le T \le 800$ K by the laser-flash technique. A thin graphite coating was applied to the surface of the pellet to maximize heat absorption and emissivity. The thermal conductivity (κ) is determined using $\kappa = \alpha \cdot C_p \cdot d$, where C_p is the specific heat and d is the sample density. Specific heat was calculated using the Dulong–Petit equation.

3 Results and discussion

3.1 Structural characterization

Preliminary characterization of $Eu_xCo_4Sb_{12}$ was performed by laboratory XRD for some pellets ground into powder; a typical XRD pattern is shown in Figure 1a. The pattern corresponds to the skutterudite structure, defined in the space group $Im\overline{3}$ (No. 204). No impurities, such as Sb, were observed in the pattern.

The high angular resolution of SXRD data was essential to thoroughly investigate the structural features of $Eu_{0.5}Co_4Sb_{12}$ nominal composition. The crystal structure was refined in the skutterudite $Im\overline{3}$ model, where Sb atoms

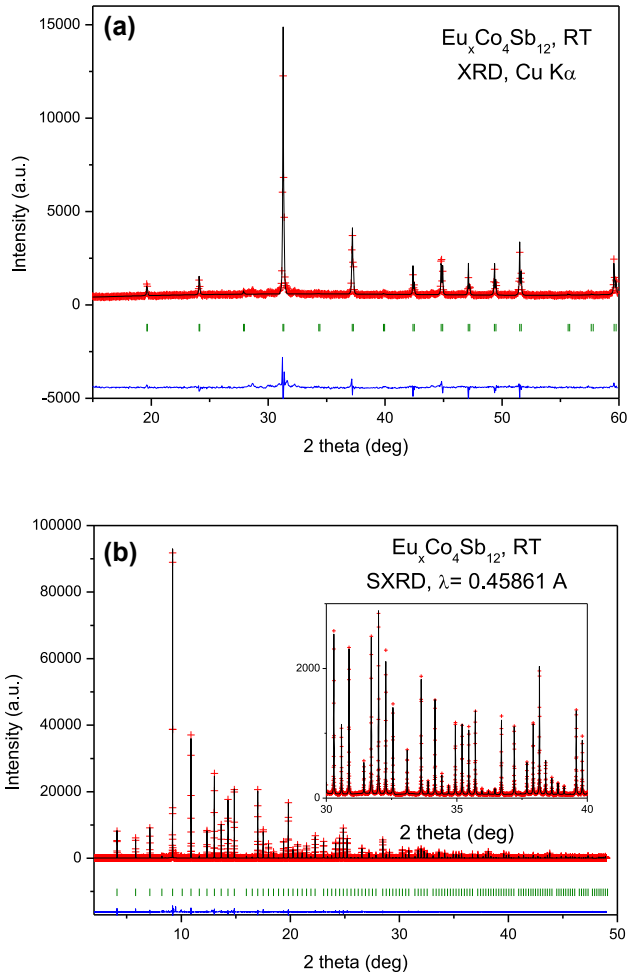

Figure 1: Rietveld plots from X-ray diffraction data: (a) Laboratory XRD pattern with Cu Kα radiation and (b) SXRD pattern for $Eu_xCo_4Sb_{12}$ at room temperature (x = 0.02(1)). The inset shows the quality of the fit in the high-angle region. Experimental points (red crosses), calculated profile (black line), difference (blue line), and Bragg reflections (green symbols).

are located at 24*g* (0, *y*, *z*), Co at 8*c* (¼, ¼, ¼) and Eu was preliminary set at 2*a* (0, 0, 0) Wyckoff positions. An excellent fit to the 295 K pattern was reached, as illustrated in Figure 1b, with unit cell parameter a = 9.03648(2) Å. However, the refinement of the Eu occupancy factor at 2*a* sites invariably converged to a slightly negative value (f_{occ} = −0.017), indicating that the rattling atom was not located at this position. Difference Fourier maps from the unfilled skutterudite framework $CoSb_3$ and the experimental SXRD data, showed conspicuous peaks of positive density at 12*d* (x, 0, 0) sites, with $x \sim 0.25$, as illustrated in Figure 2a. Two additional 2D Fourier difference plots are included at the Supplementary Information (SI) as Figure S1. A full refinement of the crystal structure including Eu at 12*d* yielded positive occupancy and displacement factors. The refined Eu content is much lower than the nominal stoichiometry, with total x = 0.02(1) for nominal x = 0.5. Similar average filling levels have been described elsewhere for La-filled skutterudites [7] or Y-filled specimens [16]. Also, a slight Sb deficiency is observed after the final run; the refined stoichiometry is $Eu_{0.02(1)}Co_4Sb_{11.95(1)}$. Indeed, an even more defective Sb sublattice has been frequently observed in skutterudites prepared under high-pressure conditions [12–14]; e.g. for the unfilled specimen, a refined stoichiometry $Co_4Sb_{11.60(1)}$ was determined [12]. The final structural parameters, including anisotropic displacement parameters for Co and Sb, and agreement factors for the final refinement, are included in Table 1. The difference with the nominal Eu content can be accounted for by the presence of tiny amounts of Eu_3Sb_2, EuO and other unidentified minor impurities in the SXRD pattern (unobservable in the laboratory XRD pattern, Figure 1a). We can speculate that there is

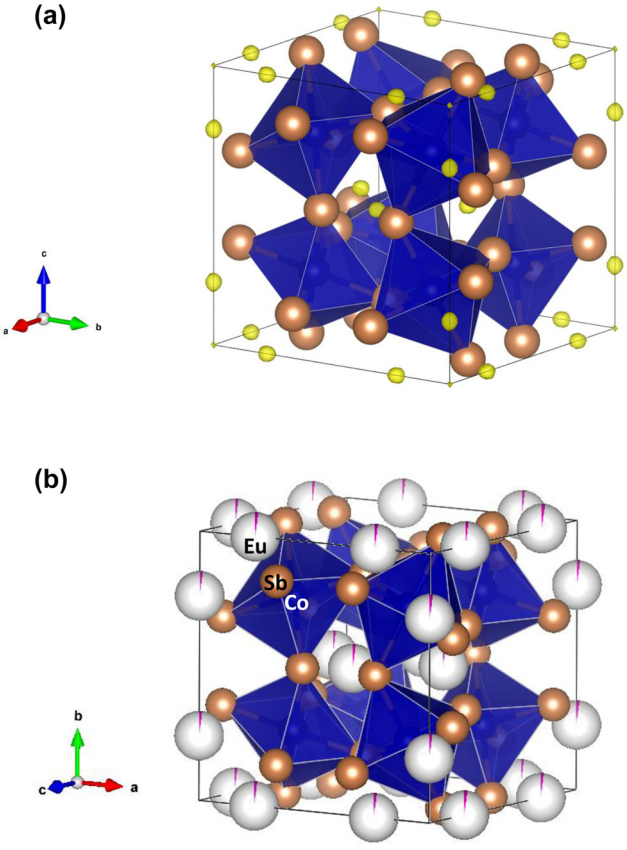

Figure 2: Views of the skutterudite unit cell: (a) Difference Fourier map showing yellow regions with positive scattering density at 12*d* sites. (b) View of the skutterudite crystal structure, consisting of a framework of $[CoSb_6]$ octahedra sharing vertices, with Eu atoms located in the large cages left in between. Eu are found to be statistically occupying 12*d* sites, conforming regular octahedra centered at 2*a* (0, 0, 0) positions.

Table 1: Structural parameters of $Eu_xCo_4Sb_{12}$ prepared under high-pressure conditions, obtained from SXRD data at 295 K.

Crystal data					
a = 9.03647(2) Å					V = 737.90(1) Å^3
Z = 2					
Refinement					
R_p = 11.79%					R_{wp} = 20.19%
R_{exp} = 5.58%					R_{Bragg} = 2.07%
χ^2 = 6.43					
Fractional atomic coordinates and isotropic or equivalent isotropic displacement parameters (Å^2)					
	Site	***x***	***y***	***z***	U_{iso}*/U_{eq}	**Occ. (<1)**
Co	8*c*	1/4	1/4	1/4	0.0060(4)	
Sb	24*g*	0	0.33488(7)	0.15792(7)	0.0077(4)	0.996(4)
Eu	12*d*	0.23(2)	0	0	0.02(1)*	0.0033(18)
Atomic displacement parameters (Å^2)						
	U^{11}	U^{22}	U^{33}	U^{12}	U^{13}	U^{23}
Co	0.0060(4)	0.0060(4)	0.0060(4)	0.0004(5)	0.0004(5)	0.0004(5)
Sb	0.0067(3)	0.0089(4)	0.0075(4)	0.00000	0.00000	0.0009(3)

a thermodynamic equilibrium that requires an excess of filler to achieve a certain filling fraction.

Figure 2b displays a view of the $Eu_xCo_4Sb_{12}$ crystal structure, highlighting the framework of corner-sharing, heavily tilted [$CoSb_6$] octahedra. The Eu atoms were found statistically distributed at high multiplicity 12*d* sites, with a weak occupancy. This contrasts with the usually described filling of the 2*a* cages in skutterudites, in oversized cages where the filler elements are described to rattle, thus acting as a sink for phonons and, therefore, drastically reducing the lattice component of the thermal conductivity. In the present case, the Eu filler is also in this cage but it is found to be out of center, delocalized in an octahedral configuration within the cavity left in between each 8 [$CoSb_6$] octahedra. This configuration determines two types of Eu–Sb distances, at 1.71(1) and 3.10(1) Å. It is evident that the first distance is unrealistic, but considering the weak Eu occupancy and the Sb vacancies in the structure, we can accept that the Eu presence in a certain position is coupled to a Sb vacancy, and thus, supporting this arrangement.

3.2 Thermal evolution

The thermal evolution of the crystal structure was determined from temperature-dependent SXRD patterns collected at 473, 673, 873 and 1023 K. The skutterudite framework is preserved up to 873 K, exhibiting the expected thermal expansion. Eu is located at 12*d* sites at 473 and 673 K, but at 873 K the Eu occupancy fades down. This reduced filling fraction reveals a segregation of the rare-earth element from the skutterudite framework, and it indicates a thermally activated reorganization of the atomic structure at high temperature, revealing the metastable nature of this compound prepared under high-pressure. Table S1 at the Supplementary Information includes the main structural parameters above RT, and Figure S2 illustrates the quality of the fits to the SXRD patterns at these temperatures. Finally, at 1023 K, a total decomposition of the skutterudite structure is observed, to give a mixture of Sb and $CoSb_2$.

3.3 Debye model

Although the mean-square displacements (MSDs) of the Eu atoms were not properly derived from the Rietveld refinement, we have evaluated the lattice dynamics of $Eu_{0.02(1)}Co_4Sb_{12}$ by following the thermal dependence of the anisotropic displacement parameters u_{ij} (in units of Å^2) of Co and Sb atoms. The dynamic contribution to the MSDs can be described using the Debye model [24], as expressed below:

$$u_{ij} = \frac{3\hbar^2 T}{m k_B \theta_D^2}\left[\frac{T}{\theta_D}\int_0^{\theta_D/T}\frac{z}{e^z-1}dz + \frac{\theta_D}{4T}\right] + d_s^2 \qquad (1)$$

such that, θ_D represents the Debye temperature, m is the atomic mass, d_s^2 denotes the static disorder, T is the

absolute temperature, and ($\hbar$, k_B) maintain their usual meaning in physics. Besides, the components u_{ij} were diagonalized to provide information on the displacements along the principal axes. The Co atoms are at 8*c* sites, which are more symmetric than sites 24*g* of Sb atoms. For such a reason, the tensor u_{ij} of Co has two independent components u_x and $u_y = u_z$, while for Sb the tensor u_{ij} presents three independent components, namely u_x, u_y, and u_z. From these values, the isotropic displacement parameters $u_{iso}^{Co} = (u_x + 2u_y)/3$ and $u_{iso}^{Sb} = (u_x + u_y + u_z)/3$ were used to estimate the Debye temperature (θ_D) of the $Eu_xCo_4Sb_{12}$ by averaging the isotropic displacements by the atomic masses of Co and Sb atoms. Then, the estimated value of θ_D was 273(2) K, which is in good agreement with the previously reported values in literature for $CoSb_3$ [12].

The evaluation of the Debye temperature along diagonal elements of u_{ij} can provide information on the vibrational properties and lattice dynamics more precisely than a simple estimation using the isotropic displacement parameters. Figure 3 displays the thermal evolution of the anisotropic displacements factors for Co and Sb atoms. For Co atoms, the Debye temperature from u_x was θ_D = 359(2) K, while that value from $u_y = u_z$ was θ_D = 402(2) K. It means that u_x is a parallel vibration along the bond Co–Sb because this value agrees with the Einstein temperature estimated from EXAFS analyses (θ_E = 345 K) [25]. For Sb atoms, the Debye temperatures from u_x, u_y, and u_z were 208, 244, and 264 K, respectively. It denotes that u_x and u_y represent displacements along the bonds d_1 (short Sb–Sb bond) and d_2 (long Sb–Sb bond) of the [Sb_4] rings, since their Debye temperatures are in good agreement with the values also extracted from EXAFS data [25]. The lattice properties coming from the framework of corner-sharing [$CoSb_6$] octahedra seem not to be dramatically affected by the presence of Eu atoms at interstitial sites, maintaining their Debye energies almost unchanged as compared to the pristine $CoSb_3$.

3.4 Oftedal plots

As mentioned, the $CoSb_3$ skutterudite structure (Figure 2b) mainly consists of a framework of corner-sharing [$CoSb_6$] octahedra, so severely tilted that Sb atoms are at bonding distances in rectangular [Sb_4] rings (Figure 4a). Therefore, there are two main covalent interactions: one between Co and Sb atoms, in [$CoSb_6$] units, and the second one between every four Sb atoms, in the mentioned rings. These rings are characteristic of this type of structure [26], and the size and degree of distortion

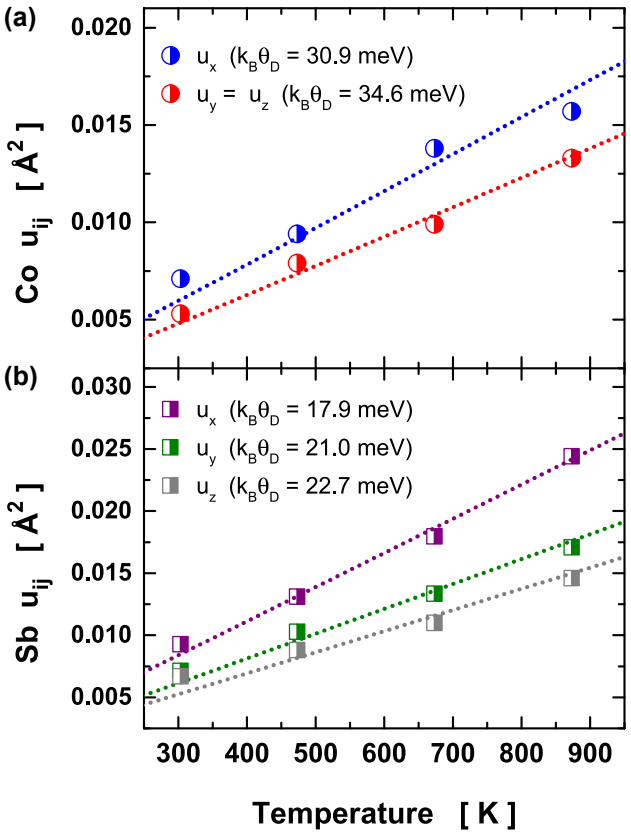

Figure 3: Temperature dependence of the diagonal elements of the anisotropic displacements u_{ij} for (a) Co and (b) Sb atoms. The dotted lines are the best fits to the experimental data using the Debye model. The standard deviations are much smaller than the size of the symbols. *Abbreviations*: $\varepsilon_D = k_B\theta_D$ is the Debye energy.

from the perfect square shape are determined by the *y* and *z* Sb positional parameters. The covalent interactions among pnictogen atoms have been analyzed in several works in terms of the electronic properties of the material, and this interaction is closely related to the band gap and valence band representation [19, 26].

As a consequence of the framework symmetry, there are only three main parameters to specify the structure: the lattice parameter ***a***, and *y* and *z* atomic positions of Sb, besides the filling fraction (FF) or occupancy of the filler M atom (*x*). Figure 4b displays the evolution of the lattice parameters depending on the filling fraction of the 2*a* positions. This plot includes precedent materials prepared under the same high-pressure conditions, containing La, Ce, Sr, K, and Yb as filler elements [12–16]. All of them have been investigated by SXRD. The labels indicate the refined occupation of the filler. The main trend is a linear behavior with the filling fraction. The present $Eu_{0.02(1)}Co_4Sb_{12}$ sample falls within this trend, slightly smaller in unit-cell parameter than $Y_{0.02}Co_4Sb_{12}$, with the same occupancy, perhaps due to the different

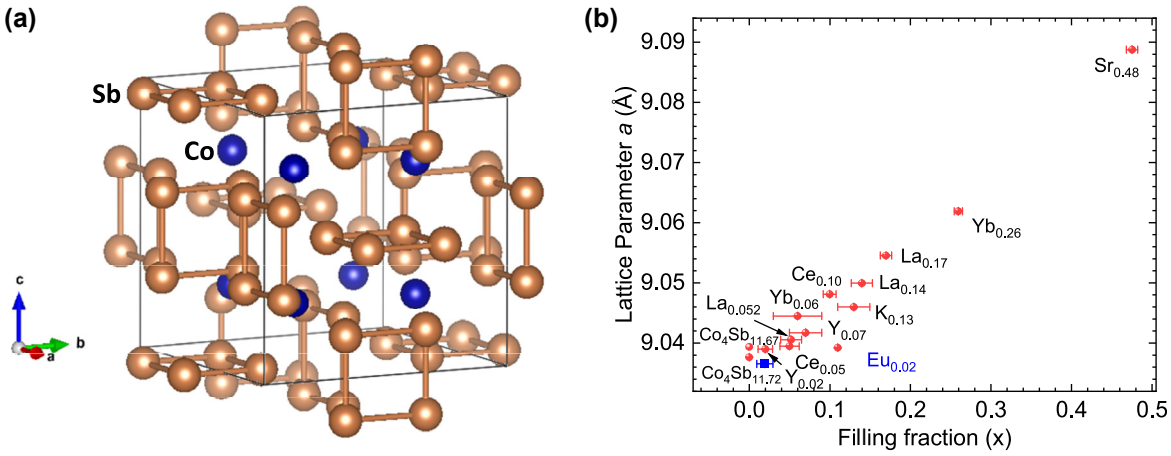

Figure 4: Features of the $Eu_xCo_4Sb_{12}$ structure: (a) [Sb_4] rings in the skutterudite structure, occurring because of the strong tilting of [$CoSb_6$] octahedra. (b) Evolution of the unit-cell parameter of the skutterudite against the filling fraction, for specimens previously synthesized under high-pressure conditions (taken from Ref. [16]), where the Eu sample falls among the slightly filled materials.

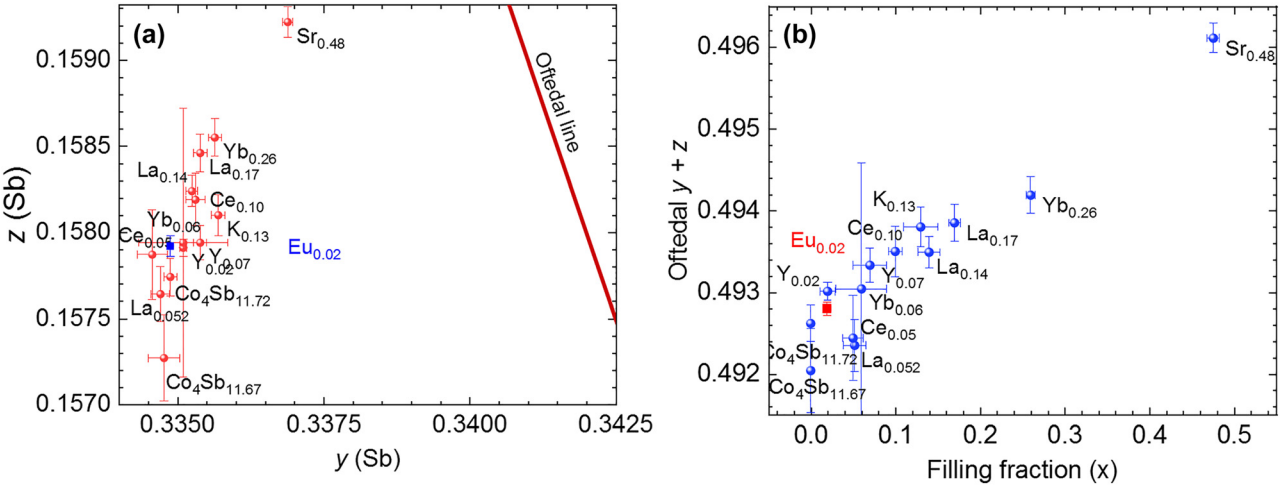

Figure 5: Oftedal analysis, including other skutterudites: (a) Oftedal plot, including the Oftedal line (red line) for $(y + z) = 0.5$ and (b) $(y + z)$ parameter against filling fraction (x or FF) for the differently filled skutterudites phases prepared under high-pressure. Single-filled skutterudite structural parameters of $M_xCo_4Sb_{12}$ (M = La, Ce, K, Sr, Yb) correspond to high-pressure samples studied from SXRD data [13, 14, 16]. $Eu_{0.02(1)}Co_4Sb_{12}$ roughly follows the observed trend.

position exhibited by the rattling element: 12*d* for Eu and 2*a* for Y [16].

Figure 5a shows the Oftedal plot with different skutterudite compositions, prepared under high-pressure conditions. The Oftedal plot consists of a representation of the z versus y fractional positions of Sb within the crystal structure. The so-called Oftedal line with $(y + z) = 0.5$ corresponds to a perfectly square [Sb_4] ring. We observed that the y and z parameters, determined from SXRD data, increase with the filling fraction, as it has been also described for other skutterudite compounds [27]. Our Eu specimen roughly falls within the observed trend regarding y and z values. Figure 5b represents the experimental $(y + z)$ parameters with respect to the filling fraction. At first glance, the $(y + z)$ magnitude behaves as the lattice parameter; however, there are important deviations. There is a pronounced effectiveness in reducing the rectangular distortion of the [Sb_4] rings as the filling fraction increases. Previous studies on the contribution of an additional electronic band to carrier transport have shown an increasing valley degeneracy and improvements in the ratio of electrical conductivity and Seebeck coefficient [28]. These indicate a direct relation of the [Sb_4] ring structural parameters with the energy difference of conduction bands. Particularly, a high band degeneracy is predicted for Sr-filled $CoSb_3$ [29], exhibiting particularly good thermoelectric properties [16, 29]. Regarding Eu, its poor filling implies

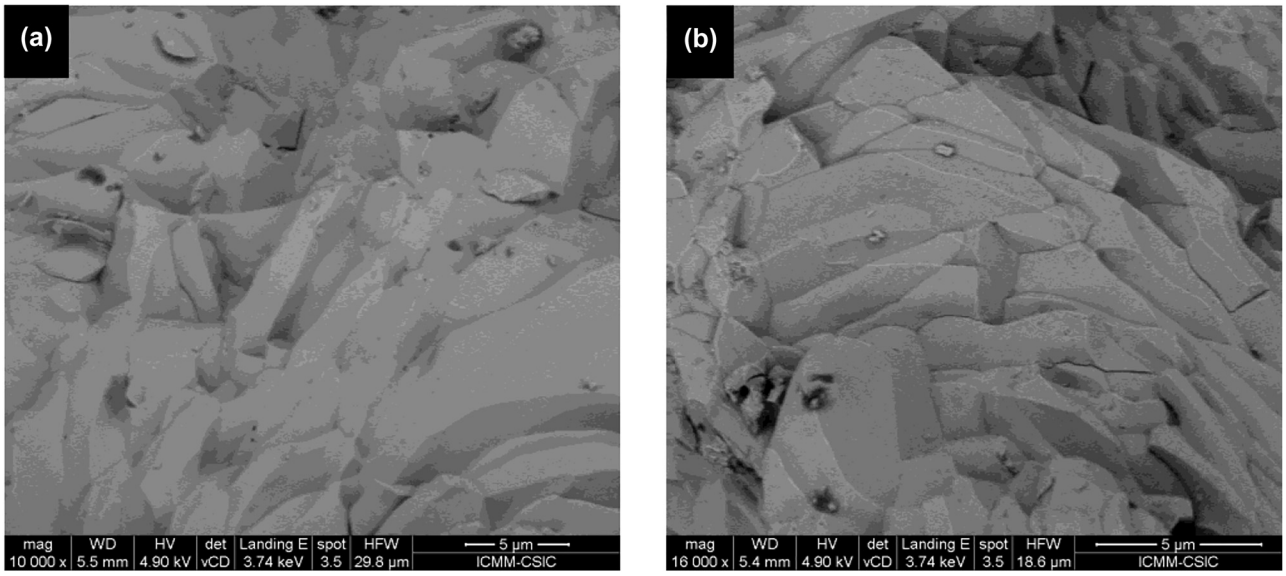

Figure 6: SEM micrographs of the as-grown pellets of $Eu_{0.02(1)}Co_4Sb_{12}$. (a) ×10,000 and (b) ×16,000 magnification.

substantially distorted [Sb_4] rings, and poor thermoelectric behavior, as described below.

3.5 Scanning electron microscopy (FE-SEM)

Grain boundary and morphology have been examined by FE-SEM to assess the compactness and homogeneity of the samples. Figure 6 illustrates two SEM images of $Eu_{0.02(1)}Co_4Sb_{12}$ sample, showing large grains above 5 µm in size, and a highly compact microstructure, as well-sintered pellets resulting from the high-pressure synthesis. Figure S3 illustrates more views of the microstructure of this sample and Figure S4 contains the results of an EDX study, yielding Eu:Co:Sb ratios similar to those expected.

3.6 Thermoelectric properties

The electrical transport properties of the $Eu_{0.02(1)}Co_4Sb_{12}$ are displayed in Figure 7a. The data of unfilled $CoSb_{3-\delta}$, $Ce_{0.5}$- and $La_{0.5}$- filled skutterudites prepared under the same high-pressure conditions [12–14] are shown for the sake of comparison. We can notice that, surprisingly, the resistivity of $Eu_{0.02(1)}Co_4Sb_{12}$ at room temperature, ~3×10^{-4} Ω m, is slightly higher than that of $CoSb_3$. However, the resistivity of the Eu-doped filled compound is closer to that of $Ce_{0.5}Co_4Sb_{12}$ as temperature increases, reaching a minimum of 5.2×10^{-5} Ω m at 750 K.

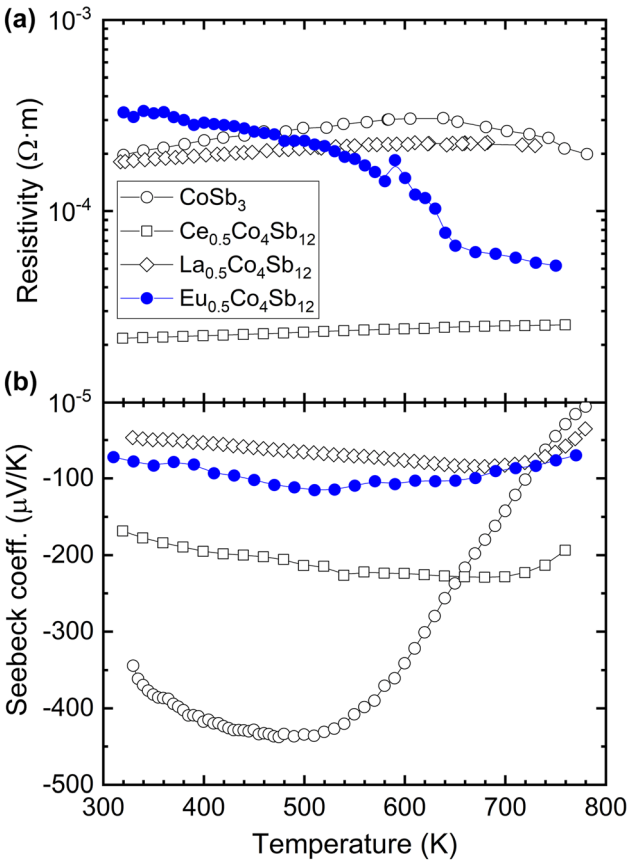

Figure 7: Temperature dependence of (a) resistivity and (b) Seebeck coefficient of $Eu_{0.02(1)}Co_4Sb_{12}$. The additional compositions, in their nominal chemical formula, have been added for the sake of comparison, namely $CoSb_3$ and $M_{0.5}Co_4Sb_{12}$ (M = La, Ce).

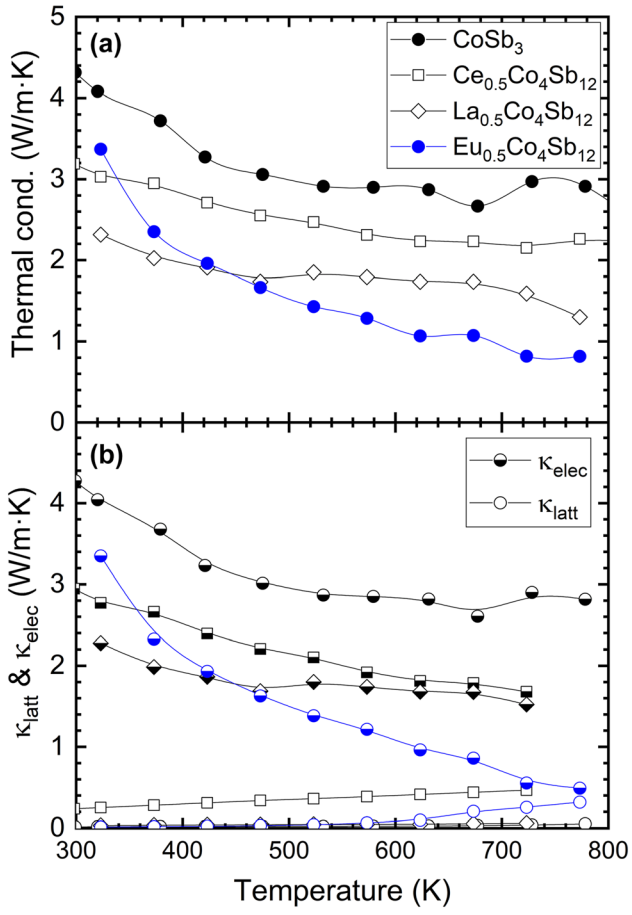

Figure 8: Temperature dependence of (a) total thermal conductivity and (b) its lattice and electronic contributions for $Eu_{0.02(1)}Co_4Sb_{12}$. Additional compositions, in their nominal chemical formulae, have been added for the sake of comparison, namely $CoSb_3$ and $M_{0.5}Co_4Sb_{12}$ (M = La, Ce).

The Seebeck coefficient is plotted in Figure 7b. Such a parameter always lies between 70 and 120 μV/K throughout the entire measured temperature range, similar to other filled skutterudites [14, 30–32]. The Seebeck coefficient for $Eu_{0.02(1)}Co_4Sb_{12}$ is always higher than that measured for the La-filled compound, but it is also remarkably lower than that value for the nominal composition $Ce_{0.5}Co_4Sb_{12}$.

The thermal conductivity of $Eu_{0.02(1)}Co_4Sb_{12}$ is shown in Figure 8a, together with data, for the sake of comparison, of similar skutterudites also synthesized under high-pressure [12–14]. The thermal conductivity of Eu-filled compound is lower at all temperatures than that of the unfilled skutterudite. It is worth noting that, at room temperature, its thermal conductivity is higher than that shown by the Ce- and La- filled skutterudites, which is probably due to the lower filling fraction reached by Eu in the $CoSb_3$ structure (~0.02(1)). However, as temperature increases, the $Eu_{0.02(1)}Co_4Sb_{12}$ compound reaches the lowest thermal conductivity compared to the other compositions prepared by high-pressure synthesis, with a minimum value of 0.82 W m^{-1} K^{-1} from 723 up to 773 K. Moreover, these are extremely low compared to other single-filled $CoSb_3$ derivatives [14, 30, 31], and thus, suggests a stark phonon scattering enhancement due to the distinctive crystallographic position of Eu atoms at 12*d* sites coupled with Sb vacancies. In fact, Eu-filled $CoSb_3$ prepared by conventional methods still show lower lattice thermal conductivity at high temperature than other filled $CoSb_3$, slightly above that reported here [33].

The two different contributions to the thermal conductivity, the lattice and the electronic parts, are displayed in Figure 8b. We can see that they follow the same trend than the total thermal conductivity, reaching a minimum value at 773 K. It can also be noticed that, for the case of $Eu_{0.02(1)}Co_4Sb_{12}$, the electronic contribution is only relevant beyond 600 K, when the electrical resistivity of the compound is lower enough. Moreover, beyond this temperature it is when the Eu-filled skutterudite shows its highest thermoelectric figure of merit, ZT, reaching a value of ~0.12 at 723 K (see Figure S5). This maximum is superior than that observed in the $La_{0.5}Co_4Sb_{12}$ nominal composition prepared under high pressure, owing to its lower resistivity with respect to that of the La-filled compound beyond 550 K.

4 Conclusions

The synthesis and sintering of $Eu_{0.02(1)}Co_4Sb_{12}$ skutterudite was carried out in one step under high-pressure conditions, followed by quenching. The structural analysis from SXRD data discloses a novel position for the rattling Eu atoms, at 12*d* sites within the large overdimensioned cages occurring in the skutterudite framework. The Debye temperature was obtained by averaging the isotropic displacements by the Co and Sb atomic masses, providing θ_D of 273(2) K. The structural data have been analyzed in terms of the Oftedal plots, compared to other M-filled specimens prepared under high-pressure conditions. FE-SEM micrographs display large and well-connected grains in a compact matrix stabilized under the synthesis conditions. The thermoelectric properties yield a Seebeck coefficient around ~70–120 μV/K throughout the whole temperature range, which leads to an enhanced power factor compared to the unfilled $CoSb_3$. The rattling effect of Eu is responsible for a substantial reduction of the

thermal conductivity to values as low as 0.82 W m^{-1} K^{-1} at 773 K, resulting in a thermoelectric figure of merit ZT ~ 0.12 at 723 K.

Acknowledgements: All the authors thank the Spanish Ministry for Science and Innovation (MCIN/AEI/10.13039/501100011033) for funding the project numbers: PID2021-122477OB-I00 and TED2021-129254B-C22. J.G. thanks MICINN for granting the contract PRE2018-083398. The authors wish to express their gratitude to ALBA technical staff for making the facilities available for the synchrotron X-ray diffraction experiment number 2017072260.
Author contributions: All the authors have accepted responsibility for the entire content of this submitted manuscript and approved submission.
Research funding: None declared.
Conflict of interest statement: There are no conflicts to declare.

References

1. Li J.-F., Liu W.-S., Zhao L.-D., Zhou M. High-performance nanostructured thermoelectric materials. *NPG Asia Mater.* 2010, *2*, 152–158.
2. Snyder G. J., Toberer E. S. Complex thermoelectric materials. *Nat. Mater.* 2008, *7*, 105–114.
3. Nolas G. S., Morelli D. T., Tritt T. M. Skutterudites: a phonon-glass-electron crystal approach to advanced thermoelectric energy conversion applications. *Annu. Rev. Mater. Sci.* 1999, *29*, 89–116.
4. Zhu T., Liu Y., Fu C., Heremans J. P., Snyder J. G., Zhao X. Compromise and synergy in high-efficiency thermoelectric materials. *Adv. Mater.* 2017, *29*, 1605884.
5. Slack G. A. CRC handbook of hermoelectrics. In *CRC Handbook of Thermoelectricshermoelectrics*; Rowe D. M., Ed.; CRC Press: Boca Raton, FL, 1995; pp. 407–440.
6. Qiu P. F., Yang J., Liu R. H., Shi X., Huang X. Y., Snyder G. J., Zhang W., Chen L. D. High-temperature Electrical and Thermal Transport Properties of Fully Filled Skutterudites RFe_4Sb_{12} (R_5Ca, Sr, Ba, La, Ce, Pr, Nd, Eu, and Yb). *J. Appl. Phys.* 2012, *12*, 063713.
7. Shi X., Bai S., Xi L., Yang J., Zhang W., Chen L., Yang J. Realization of high thermoelectric performance in n-type partially filled skutterudites. *J. Mater. Res.* 2011, *26*, 1745–1754.
8. Nolas G. S., Slack G. A., Morelli D. T., Tritt T. M., Ehrlich A. C. The effect of rare-earth filling on the lattice thermal conductivity of skutterudites. *J. Appl. Phys.* 1996, *79*, 4002.
9. Patschke R., Zhang X., Singh D., Schindler J., Kannewurf C. R., Lowhorn N., Tritt T., Nolas G. S., Kanatzidis G. M. Thermoelectric properties and electronic structure of the cage compounds $A_2BaCu_8Te_{10}$ (A = K, Rb, Cs): systems with low thermal conductivity. *Chem. Mater.* 2001, *13*, 613–621.
10. Koza M. M., Johnson M. R., Viennois R., Mutka H., Girard L., Ravot D. Breakdown of phonon glass paradigm in La- and Ce-filled Fe_4Sb_{12} skutterudites. *Nat. Mater.* 2008, *7*, 805–810.
11. Snyder G. J., Christensen M., Nishibori E., Caillat T., Iversen B. B. Disordered zinc in Zn_4Sb_3 with phonon-glass and electron-crystal thermoelectric properties. *Nat. Mater.* 2004, *3*, 458–463.
12. Prado-Gonjal J., Serrano-Sánchez F., Nemes N. M., Dura O. J., Martínez J. L., Fernández-Díaz M. T., Fauth F., Alonso J. A. Extra-low thermal conductivity in unfilled $CoSb_{3-\delta}$ skutterudite synthesized under high-pressure conditions. *Appl. Phys. Lett.* 2017, *111*, 083902.
13. Serrano-Sánchez F., Prado-Gonjal J., Nemes N. M., Biskup N., Varela M., Dura O. J., Martínez J. L., Fernández-Díaz M. T., Fauth F., Alonso J. A. Low thermal conductivity in La-filled cobalt antimonide skutterudites with an inhomogeneous filling factor prepared under high-pressure conditions. *J. Mater. Chem. A* 2018, *6*, 118–126.
14. Serrano-Sánchez F., Prado-Gonjal J., Nemes N. M., Biskup N., Dura O. J., Martínez J. L., Fernández-Díaz M. T., Fauth F., Alonso J. A. Thermal conductivity reduction by fluctuation of the filling fraction in filled cobalt antimonide skutterudite thermoelectrics. *ACS Appl. Energy Mater* 2018, *1*, 6181–6189.
15. Gainza J., Serrano-Sánchez F., Prado-Gonjal J., Biskup N., Dura O. J., Martínez J. L., Fauth F., Alonso J. A. Substantial thermal conductivity reduction in mischmetal skutterudites Mm: XCo_4Sb_{12} prepared under high-pressure conditions, due to uneven distribution of the rare-earth elements. *J. Mater. Chem. C* 2019, *7*, 4124–4131.
16. Gainza J., Serrano-Sánchez F., Rodrigues J. E., Prado-Gonjal J., Nemes N. M., Biskup N., Dura O. J., Martínez J. L., Fauth F., Alonso J. A. Unveiling the correlation between the crystalline structure of M-filled $CoSb_3$ (M = Y, K, Sr) skutterudites and their thermoelectric transport properties. *Adv. Funct. Mater.* 2020, *30*, 2001651.
17. Rodrigues J. E. F. S., Gainza J., Serrano-Sánchez F., Ferrer M. M., Fabris G. S. L., Sambrano J. R., Nemes N. M., Martínez J. L., Popescu C., Alonso J. A. Unveiling the structural behavior under pressure of filled $M_{0.5}Co_4Sb_{12}$ (M = K, Sr, La, Ce, and Yb) thermoelectric skutterudites. *Inorg. Chem.* 2021, *60*, 7413–7421.
18. Gainza J., Serrano-Sánchez F., Nemes N. M., Dura O. J., Martínez J. L., Fauth F., Alonso J. A. Strongly reduced lattice thermal conductivity in Sn-doped rare-earth (M) filled skutterudites $M_xCo_4Sb_{12-y}Sn_y$, promoted by Sb–Sn disordering and phase segregation. *RSC Adv.* 2021, *11*, 26421–26431.
19. Tang Y., Gibbs Z. M., Agapito L. A., Li G., Kim H-S, Nardelli M. B., Curtarolo S., Snyder G. J. Convergence of multi-valley bands as the electronic origin of high thermoelectric performance in $CoSb_3$ skutterudites. *Nat. Mater.* 2015, *14*, 1223–1228.
20. Jeitschko W., Foecker A. J., Paschke D., Dewalsky M. V., Evers Ch. B. H., Künnen B., Lang A., Kotzyba G., Rodewald U. Ch., Möller M. H. Crystal structure and properties of some filled and unfilled skutterudites: $GdFe_4P_{12}$, $SmFe_4P_{12}$, $NdFe_4As_{12}$, $Eu_{0.54}Co_4Sb_{12}$, $Fe_{0.5}Ni_{0.5}P_3$, CoP_3, and NiP_3. *Z. Anorg. Allg. Chem.* 2000, *626*, 1112–1120.
21. Fauth F., Boer R., Gil-Ortiz F., Popescu C., Vallcorba O., Peral I., Fullà D., Benach J., Juanhuix J. The crystallography stations at the Alba synchrotron. *Eur. Phys. J. Plus* 2015, *130*, 160.
22. Rodríguez-Carvajal J. Recent advances in magnetic structure determination by neutron powder diffraction. *Phys. B* 1993, *192*, 55–69.

23. Rietveld H. M. A profile refinement method for nuclear and magnetic structures. *J. Appl. Crystallogr.* 1969, *2*, 65–71.
24. Rodrigues J. E. F. S., Escanhoela C. A. Jr., Fragoso B., Sombrio G., Ferrer F. F., Álvarez-Galván C., Fernández-Díaz M. T., Souza J. A., Ferreira F. F., Pecharromán C., Alonso J. A. Experimental and theoretical investigations on the structural, electronic, and vibrational properties of $Cs_2AgSbCl_6$ double perovskite. *Ind. Eng. Chem. Res.* 2021, *60*, 18918–18928.
25. Rodrigues J. E. F. S., Gainza J., Serrano-Sanchez F., Marini C., Huttel Y., Nemes N. M., Martínez J. L., Alonso J. A. Atomic structure and lattice dynamics of $CoSb_3$ skutterudite-based thermoelectrics. *Chem. Mater.* 2022, *34*, 1213–1224.
26. Oftedal I. XXXIII. Die Kristallstruktur von Skutterudit und Speiskobalt-Chloanthit. *Z. Kristallogr.* 1928, *66*, 517–546.
27. Chakoumakos B. C., Sales B. C. Skutterudites: their structural response to filling. *J. Alloys Compd.* 2006, *407*, 87–93.
28. Hanus R., Guo X., Tang Y., Li G., Snyder G. J., Zeier W. G. A chemical understanding of the band convergence in thermoelectric $CoSb_3$ skutterudites: influence of electron population, local thermal expansion, and bonding interactions. *Chem. Mater.* 2017, *29*, 1156–1164.
29. Yelgel Ö. C., Ballikaya S. Theoretical and experimental evaluation of thermoelectric performance of alkaline earth filled skutterudite compounds. *J. Solid State Chem.* 2020, *284*, 121201.
30. Tang Y., Hanus R., Chen S., Snyder G. J. Solubility design leading to high figure of merit in low-cost Ce-$CoSb_3$ skutterudites. *Nat. Commun.* 2015, *6*, 7584.
31. Mi J., Christensen M., Nishibori E., Iversen B. B. Multitemperature crystal structures and physical properties of the partially filled thermoelectric skutterudites $M_{0.1}Co_4Sb_{12}$ (M = La, Ce, Nd, Sm, Yb, and Eu). *Phys. Rev. B* 2011, *84*, 064114.
32. Tang Y., Chen S. W., Snyder G. J. Temperature dependent solubility of Yb in Yb–$CoSb_3$ skutterudite and its effect on preparation, optimization and lifetime of thermoelectrics. *J. Mater.* 2015, *1*, 75–84.
33. Lamberton G. A., Bhattacharya S., Littleton R. T., Kaeser M. A., Tedstrom R. H., Tritt T. M., Yang J., Nolas G. S. High figure of merit in Eu-filled $CoSb_3$-based skutterudites. *Appl. Phys. Lett.* 2002, *80*, 598–600.

Supplementary Material: The online version of this article offers supplementary material (https://doi.org/10.1515/zkri-2022-0051).